

# Optical Engineering

OpticalEngineering.SPIEDigitalLibrary.org

## **Characterization of laser thermal loading on microelectromechanical systems-based fast steering mirror in vacuum**

Paula do Vale Pereira  
Matthew T. Hunwardsen  
Kerri Cahoy

**SPIE.**

Paula do Vale Pereira, Matthew T. Hunwardsen, Kerri Cahoy, "Characterization of laser thermal loading on microelectromechanical systems-based fast steering mirror in vacuum," *Opt. Eng.* **59**(5), 056109 (2020), doi: 10.1117/1.OE.59.5.056109

# Characterization of laser thermal loading on microelectromechanical systems-based fast steering mirror in vacuum

Paula do Vale Pereira,<sup>a,\*</sup> Matthew T. Hunwarden,<sup>b</sup> and Kerri Cahoy<sup>a</sup>

<sup>a</sup>Massachusetts Institute of Technology, Space Telecommunications, Astronomy and Radiation Laboratory, Aeronautics and Astronautics Department, Cambridge, Massachusetts, United States

<sup>b</sup>Facebook, Facebook Connectivity Labs, Northridge, California, United States

**Abstract.** Microelectromechanical systems (MEMS) have produced high-quality, high-bandwidth, small form factor, and inexpensive fast steering mirror (FSM) devices potentially suitable for a large variety of applications, such as image stabilization and beam pointing in satellite-based and ground-based, free-space optical communication systems. However, one outstanding question for this application is power handling. The absorption of the mirror substrate is low, but non-negligible, so the question remains of whether thermal loading from laser radiation on a MEMS mirror will deform its surface and, if so, to what extent. We show experimental results of optical performance changes due to thermal loading for MEMS two-axis FSM devices from Mirrorcle Technologies, Inc. Results and reproducible behavior are reported and compared in ambient versus vacuum conditions, where the benefits of convective cooling are absent. Finite element analyses corroborate the experimental results and show that the mirror substrate can deform due to thermal expansion imbalances. The deformation changes the focusing characteristics of the mirror, with a peak to valley defocus (second-order Zernike mode) of up to 50 nm when the mirrors are tested in ambient and up to approximately 450 nm when under vacuum. Such defocusing negatively impacts the link budget for laser-based satellite communications. © The Authors. Published by SPIE under a Creative Commons Attribution 4.0 Unported License. Distribution or reproduction of this work in whole or in part requires full attribution of the original publication, including its DOI. [DOI: [10.1117/1.OE.59.5.056109](https://doi.org/10.1117/1.OE.59.5.056109)]

**Keywords:** microelectromechanical systems; fast steering mirror; free-space optics; communication satellite; lasers.

Paper 20200058 received Jan. 16, 2020; accepted for publication May 6, 2020; published online May 20, 2020.

## 1 Introduction

A variety of laser communications, optical sensor, and imaging applications utilize fast steering mirrors (FSM) to execute precision, high speed pointing, and/or angular error rejection as part of closed-loop feedback systems.<sup>1</sup> Traditionally, commercial FSMs have come in two varieties based on their actuation mechanism: piezo electric or voice coil.<sup>2</sup> Both technologies have heritage with industry-known advantages and disadvantages. Different applications can leverage their strengths while dealing with their weaknesses.<sup>2</sup>

Emerging low cost, small size, weight, and power applications demand disruptive solutions. Reducing the cost, size, weight, and power consumption using microelectromechanical systems (MEMS) FSM(s) leads to the main investigation of this work. Recently, advances in MEMS have produced a lower cost, small form factor (2 cm × 2 cm × 1 cm), high-bandwidth electrostatic devices that have relatively simple high voltage driver requirements that consume very little power compared to piezo and voice coil-based systems.<sup>3</sup>

MEMS FSMs are a candidate for numerous applications where cost, size, weight, or power consumption are a concern. An interesting use case for these MEMS FSMs is for free-space optical communications (FSO).<sup>4</sup>

---

\*Address all correspondence to Paula do Vale Pereira, E-mail: [paulavp@mit.edu](mailto:paulavp@mit.edu)

There is a conflict between the mirror's mass (drive force for the thickness of the substrate) and the mirror's actuation frequency. Due to limitations in MEMS motor drive forces, the FSMs need to minimize the mass of the articulated mirror to achieve desirable bandwidth performance ( $>100$  Hz). This tradeoff quickly drives the MEMS motor to its design limits while simultaneously driving the mirror substrate thickness down as thin as possible. The result of such a tradeoff is FSMs with mirror diameters of multiple millimeters (1 to 8 mm) with very high first resonances (100 s of Hz to over 1 kHz). Unfortunately, this architecture has mirror substrates with very high diameter to thickness aspect ratios ( $\gg 25:1$ ). It is generally accepted that a high-quality surface figure error (SFE) is much more challenging to achieve on mirrors with higher aspect ratios.<sup>5</sup>

A problem arises when requiring high reflectivity of these FSMs. It is known that the highest reflectivity coatings in many optical bands are deposited through multilayer stacks of high- and low-index dielectric materials.<sup>6,7</sup> Inherently, these stacked materials have different coefficients of thermal expansion, which yields differential compressive stresses on the substrate with even small changes in temperature. Even when using a material of high bulk modulus and high tensile strength (e.g., single crystal silicon or silicon carbide), any compressive stress from mirror coatings will dramatically impact the SFE and degrade the optical quality of the wavefront error (WFE) in any far-field application. The main impact on the SFE caused by the compression stress due to temperature change is the second-order Zernike mode of defocus. The surface of the mirror curves monotonically, changing the focus of the reflected light. This type of surface error can be compensated for during alignment if the SFE is known and steady. If the SFE changes during operation, the focus error will also vary and can no longer be statically compensated. This means that temperature or laser power fluctuations will incur focus errors on the optical system.

This seemingly insurmountable challenge precludes the vendor/user from leveraging high-reflectivity dielectric coatings due to the compressive stresses. Therefore, the options for optical coating/reflectance are quite limited to uncoated [Si is only partially reflective at wavelengths in the visible out to short wave infrared bands (SWIR)] or metallic coatings, such as aluminum, silver, and gold. In the case of SWIR bands, the generally accepted best reflector of these is gold, with  $\sim 97\%$  reflectivity at 1550-nm wavelength light.<sup>8,9</sup>

Links requiring high optical output power to be incident on the thin mirror of a MEMS FSM could be problematic. Consider the example of 1-W optical output power (CW) and neglect all other losses in the optical system: the 1 W of optical power yields 6 mW of heat absorbed by a gold-coated mirror of only around  $100\ \mu\text{m}$  thick, which could lead to a significant temperature increase (tens of Kelvin). For mirrors of this size, the construction/assembly of the device involves epoxy bonding a mirror substrate to a flexure pedestal that is connected to thin rods adjoined to the MEMS motors. The Mirrorcle FSM we analyzed in this work (more information about the Mirrorcle MEMS mirrors can be found at Ref. 10) has thickness of  $39\ \mu\text{m}$ , diameter of 4.2 mm, and is connected through a pedestal of  $\sim 120\ \mu\text{m}$  per side (note that the cross-section is a square) and  $350\ \mu\text{m}$  height, as can be seen in the microscope and coherence scanning interferometer images in Fig. 1. The back of the mirror is etched down to decrease weight while maintaining certain structural stability. Figure 1 also shows an image from Mirrorcle explaining their actuation system.<sup>11</sup>

Zhang et al.<sup>12</sup> have performed a thermal analysis of MEMS mirrors for high energy applications using finite element analysis and performing laboratory tests. Although the mirrors in their study are micromirrors two orders of magnitude smaller than the mirrors we are analyzing, the challenges they face are similar to what we describe in this paper: high-power laser illumination will significantly increase the temperature of MEMS mirrors and may damage their surface. The authors' model and tests are performed under vacuum, meaning that the heat loss is limited to conductive and radiative heat transfers. The results show that the mirrors may get up to  $250^\circ\text{C}$  when a laser of 150 mW is reflected at their surface. At this temperature level, the surface becomes rough and the reflectivity significantly decreases (down to as little as half of the original reflectivity). The authors conclude that the best way to decrease the mirror temperature is by decreasing the thermal resistance between the mirror and the silicon base, and they suggest two methods for accomplishing that reduction: (a) increase the effective conductive heat transfer area by adding extra mounts between the mirror and the base; (b) increase the thermal conductivity of

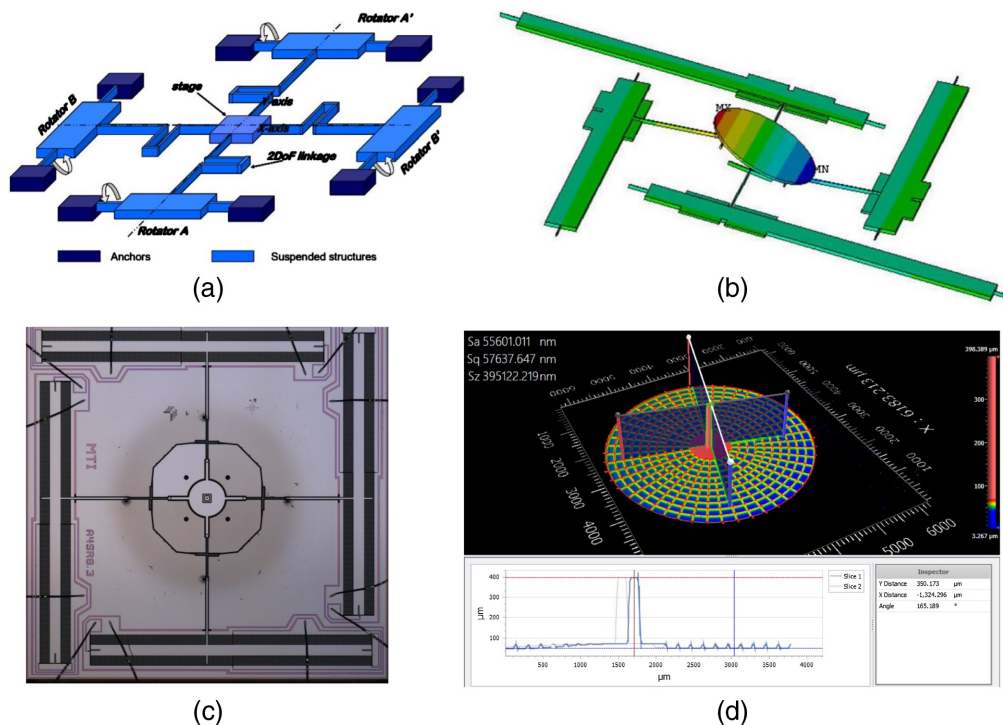


**Fig. 1** (a) FSM motor structure;<sup>11</sup> (b) FSM structure from Mirrorcle;<sup>11</sup> (c) FSM actuator structure seen through an optical microscope; and (d) mirror structure seen through a Zygo NexView2 white light interferometer.

the mounts by gold coating them. The authors mention that there is a difference in the coefficient of thermal expansion between polysilicon and gold, but they believe this difference does not pose a problem as the stiffness of silicon is higher than the stiffness of gold. Our work also involves the thermal modeling and testing of MEMS mirrors under vacuum. However, we do not believe that the thermal expansion mismatch between the mirror reflective surface and the mirror substrate can be ignored, as will be described in detail in the results section.

Similarly to Zhang et al.,<sup>12</sup> Gokce et al.,<sup>13</sup> and Wolter et al.<sup>14</sup> also suggest modifications to MEMS mirrors to improve their efficacy. Both studies suggest that a better mounting strategy of the mirror to its base can decrease the mirror's dynamic deformation, significantly improving the flatness of the mirror during operation. Gokce et al.<sup>13</sup> proposed a structure that mitigates dynamic deformation by increasing the isolation between the mirror and the flexible, dampening features. They also use a backbone structure on the back of the mirror to decrease dynamic deformation. Wolter et al.<sup>14</sup> proposed a structure with eight springs around the periphery of the mirror and demonstrates through both simulation and modeling that the structure can decrease the mean surface deformation by 80%. These two studies point out how important the flatness of a MEMS mirror is, but they do not address how temperature changes could affect the flatness.

To the best of the authors' knowledge, there are currently no papers addressing laser beam illumination thermal effects on millimeter-size MEMS FSMs. Our work closes that gap through the analysis and testing of Mirrorcle mirrors under vacuum.

## 2 Materials and Methods

A low-power 1550-nm laser source seeds a high power (0.5- to 5-W output power) erbium-doped fiber amplifier as our source laser system. We extend the power range 10× lower by adding 1.0 OD neutral density filters to the output of our laser source. This allows a testing range of irradiance from 50 mW to 5 W, or 20 dB of range (power varied from +17 to +37 dBm).

A small collimator ( $\sim 2$  to  $3$  mm diameter,  $1/e^2$ ) is used to ensure the beam is smaller than the mirror substrate diameter. Therefore, all light emitted is incident on the mirror surface. The laser beam has an angle of incidence (AOI) of  $45^\circ$  to the FSM device under test (DUT). A Thorlabs high power detector is placed at the complementary AOI to the DUT to accurately measure the power reflected off the DUT, as can be seen in Fig. 2.

The DUT is placed in the center of a custom vacuum bell jar that has three separate optical view ports, indexed at  $0^\circ$ ,  $45^\circ$ , and  $90^\circ$ . The ports at  $0^\circ$  and  $90^\circ$  deg have fused silica plano–plano flats with antireflective coatings at  $\sim 1550$  nm. The port positioned at  $45^\circ$  deg is normal to the mirror surface and has a larger zinc–selenide window. All windows, feedthroughs, and ports are sealed such that the bell jar can achieve  $3.0 \times 10^{-5}$  Torr of vacuum within a few hours when attached to a roughing/turbo pump system.

Normal to the mirror surface, we align a Zygo Dynafiz phase-shifting interferometer. This instrument measures the SFE of the mirror surface at each stage of our test procedure. The Zygo effectively looks through the zinc–selenide window, focusing on the DUT. Figure 3 shows the lab setup with the bell jar.

Lastly, at each step of laser loading, a thermal image is taken of the DUT through the zinc–selenide window with an FLIR C3 Thermal Infrared Camera to capture a qualitative measure of the mirror's surface temperature increase. The temperature measurements are only of the qualitative results, mainly due to two reasons: (i) the camera was placed outside a window, which could filter some of the infrared wavelengths that the camera uses to perform its measurements, and (ii) the mirror is coated with gold, which reflects infrared light, making it hard for the camera to distinguish between the light being reflected by the mirror and the light being emitted by the mirror.

Feedthrough ports on the bell jar provide thermocouples to mounts (it is not realistic to mount thermocouple on the mirror assembly, though) and drive signals to power the mirror under vacuum, which is very helpful for alignment and operation. The detailed test procedure is shown in Sec. 5.

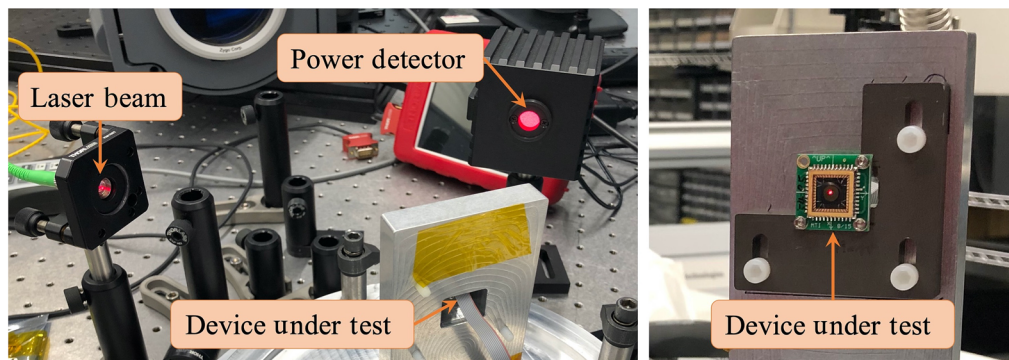


Fig. 2 Laboratory setup of the laser beam, the DUT, and the power detector.

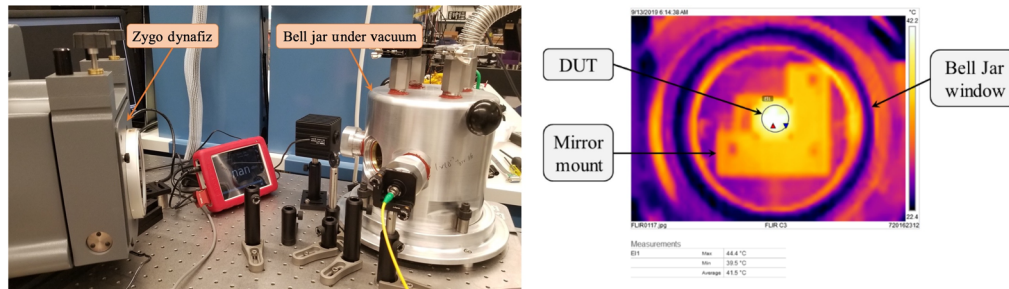


Fig. 3 Lab setup showing the bell jar under vacuum and the Zygo Dynafiz and FLIR temperature measurement showing the mirror surface temperature rise.

## 2.1 Example Data

There is a wide variance of SFE from mirror to mirror. Figure 4 shows some measurements of the SFE. Performing a Zernike decomposition shows the primary distortion is focus (optical power). This observation is true for all devices measured.

## 2.2 Observations

- Thermal effects of laser loading appear immediately as the mirror is illuminated;
- Changes in surface figure are observed immediately in the live images of the interferogram produced by the Zygo;
- The distortion asymptotes within 1 to 2 s, regardless of the laser power;
- Distortions introduced by laser loading are dominantly a focus shift, usually to increase the focal power (increase curvature).

## 3 Results

### 3.1 Thermal Problem

The size and shape of the mirror may constitute a thermal transfer problem when a laser beam is reflected on its surface. The thin substrate gives the mirror very little thermal mass (e.g., heat capacity),  $\sim 6 \times 10^{-4}$  J/K, which was calculated using the specific heat of silicon and gold and the mass of each component present in the mirror, which was calculated from the mirror dimensions, measured as described in Sec. 1, for the mirror in this study. The epoxy bond (Mirrorcle proprietary composition and properties) between the mirror and the actuation structure introduces thermal resistance, especially when compared to silicon. The thin joining flexures are also inadequately sized to transfer much heat. Considering our example case from the introduction session (a 1-W laser being reflected by the MEMS mirror surface), these devices have a very poor thermally conductive path to dissipate this constant heat load coming from the laser, as it is going to be explained in this session. Although convection is present in these devices when at normal atmosphere, the relatively small surface area of the mirror substrate ( $1.385 \times 10^{-5}$  m<sup>2</sup>) prevents convection from removing substantial amounts of heat. The low heat transfer rates through both conduction and convection cause the mirror substrate temperature to rise before reaching a thermal equilibrium. Estimations of the convection heat transfer between the mirror and the surrounding air result in only  $\sim 6$  mW when the mirror is at 50°C and 20 mW when the mirror is at 100°C.

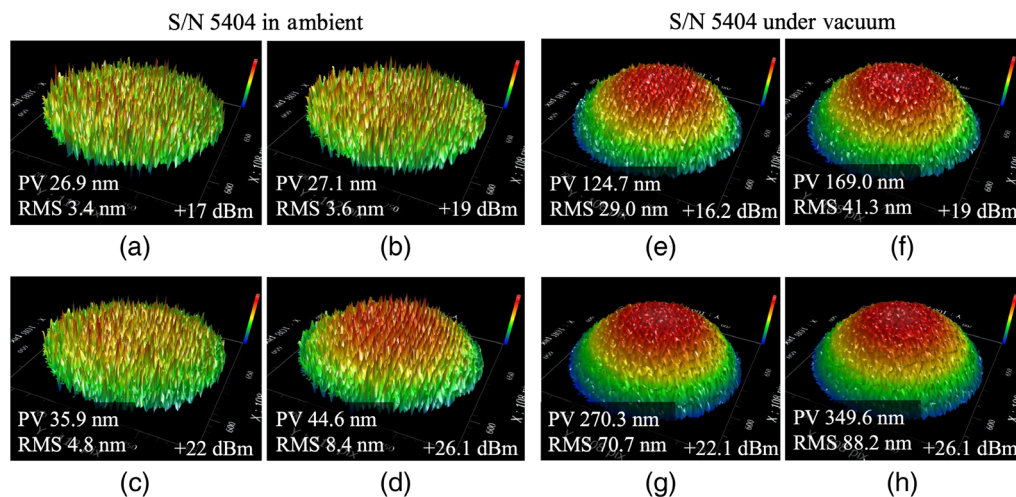


**Fig. 4** (a)–(d) Surface deformation with increasing optical power at ambient pressure. (e)–(h) Surface deformation with increasing optical power under vacuum.

Although radiative transfer of heat is present in all devices, the amount of radiative heat dissipated is very small compared to the absorbed heat. From Stefan–Boltzmann law, we analytically estimate an equilibrium temperature of 90°C and a heat radiation out of the mirror to be less than a milliwatt when a 1-W laser is reflected by the mirror surface.

Considering both convective and radiative heat extractions and an initial temperature of 22°C, a thermal analysis in Ansys calculates the mirror equilibrium to be at 33°C (+8°C above ambient) when a 0.5-W laser is reflected by its surface. The temperature rise of the mirror produces a thermal expansion mismatch between the mirror substrate and its reflective coating. This mismatch causes large stress levels in the mirror substrate, resulting in tens of nanometers of undesirable surface defocus deformation (up to 90 nm of peak to valley second-order Zernike mode deformation for a 0.5-W laser).

FSO concept of operations (CONOPS) require environments that are at or near vacuum. (At the time of this publication, the authors are aware of testing being performed by Mirrorcle on hermetically sealed versions of these MEMS devices, which emulates an atmospheric environment even when the device is under vacuum. We do not have access to the company's test results, but simulating this condition is part of our future work.) Partial to complete vacuum eliminates convection heat transfer. Without convection, the only means of thermal dissipation are conduction and radiation, which are both of low effectivity in extracting heat from the mirrors and may be difficult to implement in an FSO architecture. When an incident fluence of laser light exceeds the ability of the mirror to dissipate heat, the mirror substrate will increase in temperature, resulting in a surface deformation that degrades the SFE.

The authors believe that the heat flow can be treated mostly as unidirectional, with the temperature of the mirror being homogeneous along its surface and presenting a slope only in the normal direction (along the mirror thickness). This happens due to the high thermal conductivity of silicon and was confirmed in the finite element analysis performed in this work and depicted in Fig. 6(c).

We chose to test Mirrorcle MEMS FSMs in vacuum and use that data to validate finite element analysis results and build our model of the mirror deformation.

### 3.2 Measurements

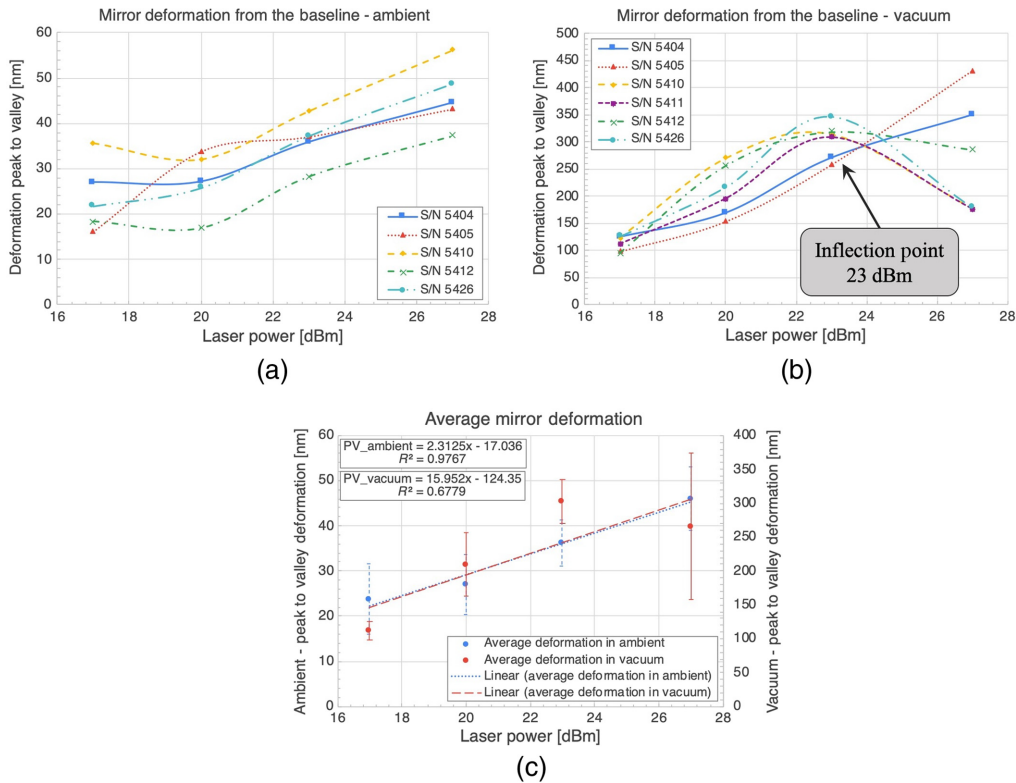
Mirrorcle FSMs show a significant deformation when the laser irradiance is incident at their surface, confirming the prediction that the heat extraction from the mirror is of low effectivity. Figure 4 shows the progression of a mirror deformation as the laser power is increased when the mirror is under ambient pressure [Figs. 4(a)–4(d)] and under vacuum [Figs. 4(e)–4(h)].

Figure 4 shows the mirror surface after a subtraction between the Zygo measurements of the mirror receiving laser power and the baseline data (no laser irradiance). The peak to valley difference in each example is annotated on the image. On all the devices we have tested, the main deformation was focus aberration (up to 430 nm of focus), showing the bowl shape that the mirrors undergo because of a CTE mismatch between the gold mirror coating and the silicon mirror substrate. Figure 3 shows the FLIR measurement of the same mirror (DUT) on the same laser power level. The mirror is gold coated and is 4.2 mm in diameter. All the mirrors analyzed for this paper have the same diameter, the same type of coating, and presented this bowing effect.

A summary of the measurements can be seen in the graphics in Fig. 5. The graphic in Fig. 5(a) contains the data measured in ambient pressure, the graphic in Fig. 5(b) contains the data measured under vacuum, and the graphic in Fig. 5(c) shows the average of the measurements, their standard deviations, and a linear trend of the peak to valley deformations. Table 1 also shows the average of the measurements in ambient and vacuum and the standard deviation of the measurements. The ambient measurements show that convection heat transfer is key in keeping the mirror at low temperatures, as the measured deformation is not significant.

The measurements under vacuum show that the deformation is significant, with a maximum of peak to valley difference from the baseline ranging from approximately 150 to nearly 450 nm. All the mirrors show a similar increase of deformation with power until 23 dBm (200 mW).

We then performed reverse-engineering measurements of one gold-coated mirror sample of 4.2 mm diameter that had failed during high-power laser testing. We used an optical microscope and an interferometer to measure the diameter and thickness of the mirror, the height, width,



**Fig. 5** Measurements of the peak to valley defocus deformation at different power levels when the mirror is under (a) ambient pressure and (b) vacuum; (c) average of the measurements and standard deviation at each power level and linear regression of the deformation as a function of the power level.

**Table 1** Average deformation of the mirrors when laser is reflected by their surface.

Power level (dBm)	Average deformation in ambient (PV nm)	Standard deviation in ambient (PV nm)	Average deformation in vacuum (PV nm)	Standard deviation in vacuum (PV nm)
17	23.74	7.80	112.45	13.75
20	27.09	6.63	209.63	46.56
23	36.22	5.17	302.41	32.72
27	46.00	7.02	265.97	108.22

and location of the mirror’s backside structure, and the width and height of the mirror’s pedestal. We used the measurements to make a CAD model of said mirror, which is shown in Figs. 6(a) and 6(b). The modeled mirror includes the mirror substrate made of silicon and the coating made of gold.

We used this geometry to model the deformation on a thermomechanical multiphysics finite element analysis on the Ansys software. For the thermal problem, we set the boundary condition for all surfaces as thermally insulated, except for the reflective mirror surface, which received the laser power. We considered the surfaces insulated because convection under vacuum and radiation at relatively low temperatures (<100°C) are negligible. The ambient temperature was set to be at 25°C. This thermal problem allows conduction between the mirror surface, the mirror substrate, the pedestal, and the actuating structure. It also allows temperature gradients in three dimensions. The results show that the laser illumination raises the temperature of the mirror surface and substrate from 25°C to 70°C, and that this raise is homogeneous, i.e., there is

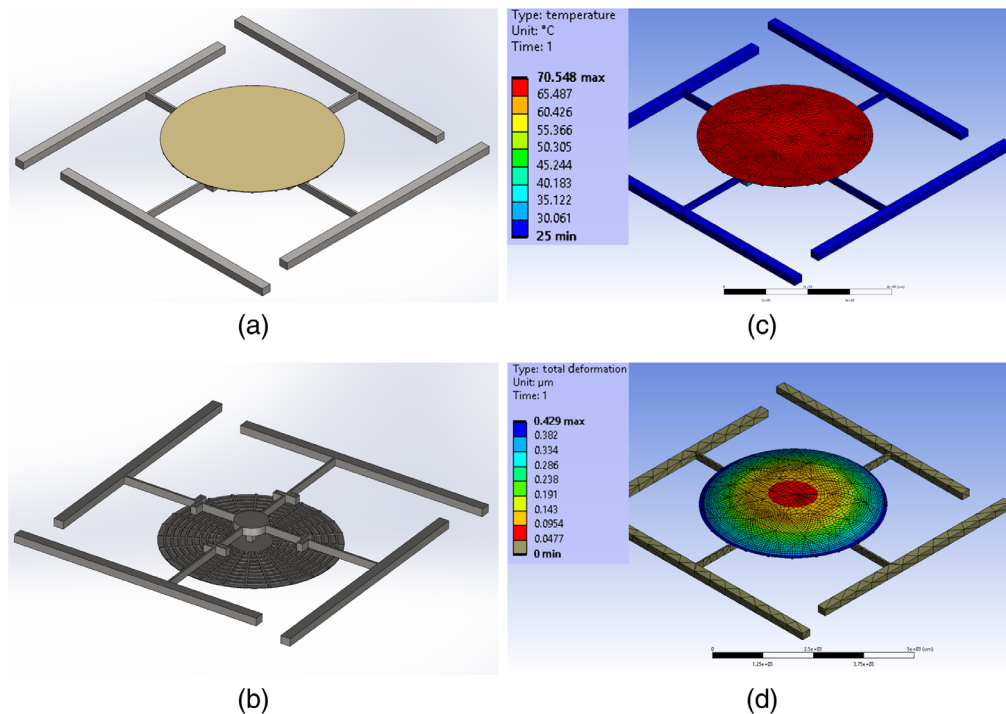


**Fig. 6** (a), (b) CAD derived from mirror reverse engineering, (c) temperature results from the Ansys thermomechanical analysis, and (d) deformation results from the Ansys thermomechanical analysis.

no gradient either on the radial or on the axial directions [Fig. 6(c)]. Both the gold coating and the silicon substrate present the same final temperature. This is expected, as gold has a high thermal conductivity and the thermal resistance between the gold and the silicon is negligible. The pedestal, however, has a cross-sectional area of only  $0.04 \text{ mm}^2$ , allowing very little heat to conduct through it. At steady state, the entire temperature drop is at the pedestal: the end attached to the mirror reaches  $70^\circ\text{C}$  and the end attached to the actuating structure stays at  $25^\circ\text{C}$ .

The results of the thermal analysis served as input into a mechanical deformation analysis. For this analysis, the edges of the actuation structure were considered fixed and the rest of the geometry was allowed to move. The resulting shape of the mirror was a bowl-like structure with maximum deformation of  $430 \text{ nm}$ , with the gold coating having expanded significantly more than the silicon substrate [Fig. 6(d)]. The other parts of the mirror structure (the pedestal and the actuation structure) did not suffer any significant deformation. The model results match the deformation measurements and temperature estimations from the laboratory experiments, namely, up to  $60^\circ\text{C}$  and  $431 \text{ nm}$  defocus deformation.<sup>15</sup> This agreement in results shows that the main source of the deformation is indeed the differential expansion due to temperature increase.

## 4 Discussion

As can be seen in Figs. 4 and 5, the total peak to valley deformation of the mirrors when a laser beam is reflected by their surface can be significant (up to  $431 \text{ nm}$ ). Mirrors in both conditions (ambient and vacuum) exhibit an increase in deformation levels as the laser power increases. As can be seen in Fig. 5(c), the average behavior in ambient pressure can be expressed as a linear trend, but the average behavior in vacuum is poorly represented by a linear regression, with an  $R^2$  of 0.68.

The standard deviation of the measurements is not negligible: it is as high as 32% for the ambient condition [ $(23.74 \pm 7.8) \text{ nm}$  for the  $17\text{-dBm}$  laser power level] and 40% for the vacuum condition [ $(265.97 \pm 108.22) \text{ nm}$  for the  $27\text{-dBm}$  laser power level], as can be seen in Table 1.

The standard deviation for the high-power test under vacuum is the highest ( $\pm 108.22$  nm), with the measured peak to valley differences ranging from 175 to 431 nm. This difference in behavior of the mirrors under vacuum at 27 dBm of laser power was not expected and we believe is caused by plastic deformations on the mirror structure which lead into the inversion of deformation direction that is explained in the anomaly's Sec. 4.3. Further tests at different laser power levels could reveal at which point this deformation starts. We also believe that this large standard deviation could be caused by differences in manufacturing because the mirrors with sequential serial numbers tend to behave extremely similarly among each other, but differently from the other pairs, as can be seen when comparing the pair  $S/N$  5404 – 5405 versus the pair  $S/N$  5411 – 5412 in Fig. 5(b).

The nonlinear trend under vacuum and the large deviation between samples make the mirror behavior hard to predict. The average behavior is similar in ambient and vacuum as in both cases the deformation increases with an increase in laser power, but we could not derive a strong correlation to predict how a mirror will behave under vacuum based on the measurements performed in ambient pressure.

#### 4.1 Impact on Link Budget

The satellite communication industry is expanding from the radio wave spectrum into the laser spectrum, using FSO communication to deliver a higher data rate using the same amount of power.<sup>16</sup> However, the pointing of optical communication systems is more challenging than the typical radio systems. One possible solution that is being used by many satellites is placing an FSM in the receiver system, which corrects for fine pointing.<sup>17</sup> A focus degradation caused by the FSM deformation could impact the link budget of such satellite communication fields. To quantify that impact, we made two analyses: WFE impact and collimation impact. In this paper, we opted for a generic impact analysis, but more case-specific analysis for projects using Mirrorcle MEMS mirrors should be performed using an optical design software, such as Zemax.

##### 4.1.1 Wavefront error impact

To consider how much the point spread function of the laser beam is affected by the WFE introduced by the mirror deformation, we use a calculation of the Strehl ratio to quantify the impact to an FSO link due to an increased (uncorrected) SFE. For low-order Zernike polynomials, including the second-order defocus (the main aberration introduced by the mirror deformation), the Strehl ratio can be defined as<sup>18,19</sup>

$$SR = \frac{1}{\exp(\sigma_\phi^2)}, \quad (1)$$

where  $\sigma_\phi$  is the residual phase variance and can be expressed as  $2\pi WFE$ , where WFE is the wavefront error as a function of the wavelength. The worst-case defocus deformation measured was on the order of 400 nm (RMS), resulting in a WFE of 0.258 waves (The WFE is defined as the peak to valley deformation in nanometers divided by the laser beam wavelength in nanometers. In this case,  $WFE = 400/1550 = 0.258$ , which means the deformation magnitude is  $\sim 25\%$  of the wavelength of the light reflecting on the deformed surface.) for a laser beam at 1550 nm. The loss on the link budget was then calculated through Eq. (2)<sup>18</sup> to get a value in decibels:

$$Loss_{\text{Focus}} = 10 \log_{10} \left[ \frac{1}{e^{(2\pi WFE)^2}} \right]. \quad (2)$$

The maximum calculated loss was of 11.42 dBm.

##### 4.1.2 Collimation impact

In a baseline situation without the defocusing aberration from the mirror and assuming the laser beam is collimated and traveling in the far-field, diffraction will unavoidably cause the beam to

enlarge after it leaves an aperture. The diameter in the far field,  $D$ , can be calculated by the Gaussian beam expansion as<sup>20</sup>

$$D = 2.44 \frac{\lambda}{d} L, \quad (3)$$

where  $d$  is the diameter of the limiting optical aperture,  $L$  is the path length, and  $\lambda$  is the wavelength of the laser beam. In a sample case, we assume an aperture diameter of 10 cm and a path length of 1000 km, resulting in a far-field diameter of 37.8 m. Due to the ratio of the transmission area to the collection area, if one was to assume 1 W (+30 dBm) was emitted from the transmitting terminal, only 0.007 mW, or -21.55 dBm, would reach a receiving aperture of 10 cm diameter in this baseline example (no mirror deformation). This means a low-power signal will arrive at the receiver even at the baseline case. This power level will decrease even more when the defocusing deformation is introduced, making it even harder for the satellite engineers to close a communication budget.

When the mirror deformation is introduced, the beam divergence increases proportionally. To calculate the divergence angle, we calculate first the focal length resulting from the defocus, as<sup>21</sup>

$$f = -\frac{\sqrt{3}\omega_0^2}{12WFE\lambda}. \quad (4)$$

The resulting focal length for a 10-cm diameter aperture and 0.258 waves of wavefront (peak to valley at 1550 nm) error is 902.335 m. The resulting divergence angle, calculated through  $\theta = d/f$ , is 110.82  $\mu$ rad.

It is common to measure beam quality using the  $M^2$  factor, which represents how much the divergence of a beam deviates from a perfect Gaussian beam and, for defocus aberration, can range from almost no influence (barely above 1) to close to 10.<sup>22-24</sup> The  $M^2$  factor can be calculated from the divergence angle using its defining equation  $\theta = (2M^2\lambda)/(\pi d/2)$ .<sup>25</sup> For the previously calculated value of  $\theta$  (110.82  $\mu$ rad), the  $M^2$  factor results in 2.81. The far-field diameter at 1000 km path length becomes 110.82 m (almost three times larger than the 37.8-m baseline case). Due to the ratio of the transmission area to the collection area, only 0.00081 mW, or -30.90 dBm, would reach a receiving aperture of 10 cm diameter.

The difference between the received power without defocusing (-21.55 dBm) and the received power with defocusing (-30.90 dBm), representing the loss caused by the mirror deformation, is 9.35 dBm.

### 4.1.3 Overall impact

Both analyses (WFE and collimation impact) result in losses of the same order of magnitude:  $\sim 10$  dBm. This shows that the mirror defocus deformation can hinder the communication link closure if this factor is not taken into account during the design phase, as normally link margins for small satellites are on the order of 3 dB.<sup>26</sup>

## 4.2 Other Potential Impacts

The usage of MEMS devices is also becoming increasingly popular in other technology fields, such as the microphone of mobile phones and voice-controllable home systems. A group of researchers from the University of Michigan has proven that these microphones can be controlled using laser light.<sup>27</sup> They pulsed a laser beam on the microphone to mimic sound waves. The authors illuminated the home systems' microphones with a 60-mW, 450-nm wavelength-pulsed laser beams, which mechanically deformed the MEMS microphone diaphragm.<sup>27</sup> This pulsed deformation would then mimic sound waves. Although the authors mentioned photoacoustic effects, they did not propose a theory for what would cause this phenomenon. We believe the microphone's diaphragm is behaving similarly to the mirrors we tested in this study: they are being deformed by the thermal stress induced by the absorbed laser light.

High-power laser applications require special coatings with high reflectivity not to overheat. One typical solution is the use of dielectric stacks of films of high and low index materials, which can reach reflectivity levels of above 99%.<sup>6</sup> The fabrication of such stacks is done through the deposition of one layer at a time, all occurring under elevated temperatures (above 40°C) and, sometimes, each occurring at a different temperature. Each layer has a different coefficient of thermal expansion, so the final optical component presents residual stress when at ambient temperature.<sup>28</sup> Many studies have been done in order to calculate this residual stress and to overcome it through to postdeposition thermal treatment.<sup>29,30</sup> We believe that the effects we describe in this paper are of similar nature to the ones encountered in the high reflectivity coatings field, which strengthens our hypothesis that the cause for MEMS mirrors defocus deformation is thermal stress.

Besides the surface defocus deformation, thermal stresses might pose at least three additional challenges when using these mirrors for FSO: variation in the surface reflectivity, coating degradation, and usage of polymers above their glass transition temperature. Minissale et al.<sup>31</sup> showed that not only gold but also other common optical materials present small variations in reflectivity with temperature, which might become significant for large temperature fluctuations. Some polymers have relatively low glass transition temperatures (below 100°C), so they may fail when the mirror structure temperature rises above that level. We experienced that phenomenon in our tests, when some of the mirrors failed on the epoxy, which delaminated from the pedestal, detaching the mirror from its structure.

### 4.3 Anomalies

#### 4.3.1 Focus sign shift

An anomaly was observed on multiple DUT's where the sign of the focus term (direction of the bowl) will change after removing laser power. We believe the thermal strain produced by the CTE mismatch causes plastic deformations on the mirror, resulting in a permanent shape change. Even with such flipping behavior, the mirrors still present repeatability: some mirrors were tested two or three times and presented similar levels of deformation at the same laser power level on all the cycles.

#### 4.3.2 Mirror failures

At higher laser levels in vacuum, numerous devices had their mirror substrate fall off. This issue is more prevalent with smaller diameter mirrors (4.2 mm) and not observed on larger diameter mirrors (7.5 and 8.2 mm). For the smaller mirrors, vendor data sheets indicate that the maximum irradiated power is 2 W. During this test campaign, we observed that many 4.2-mm diameter mirrors fail at or around the 2-W laser loading level. The mirror appears to delaminate from the pedestal, and gravity pulls the substrate off the assembly. We believe the likely causes of these failures are:

1. The structural epoxy exceeds its glass transition temperature, causing it to reflow with delamination;
2. The differential expansion from the mirror substrate and the epoxy bond cause delamination.

Even though most of the DUTs exhibited one or both of those anomalous behaviors (focus sign shift and/or mirror failure), they happened after good measurements had already been performed, resulting in low impact on the collected dataset. The understanding of such anomalies would benefit from more tests and analysis, but those are out of the scope of this paper.

### 4.4 Proposed Mitigation Strategy

To mitigate the impact of the thermal loading, we propose to also coat the back side of the mirror substrate with gold to balance the compressive stress of the mirror. Based on finite element

modeling predictions, it is anticipated that most of the thermally induced focus shift will be mitigated.

The optimal mitigation would be a redesign of the mirror substrate light weighting structure: the light weighted shape that best reduces the weight of mirrors without impacting the structural integrity and stability is well known and is different from the shape present in the Mirrorcle devices. The shape presented in the Mirrorcle devices is composed of radial and circular concentric beams, whereas the optimal shape to minimize thermal loading is a honeycomb structure.<sup>32-34</sup>

Hermetic sealing the mirrors in a small container filled with dry, inert gas will improve a MEMS FSM's ability to dissipate heat as it will keep convective heat transfer present in the sealed environment even when the outside environment is subjected to vacuum. This approach will require an optical quality window with antireflective coating on both sides. Also, one would prefer this window to be mounted at a wedged angle to suppress residual reflections. Similar solutions are available or being explored by the vendor, although application-specific solutions will drive cost and complexity.

A focus adjust/offload element added to the light path can compensate for the focus introduced by thermal loading along with effective focal length changes of an optical train due to temperature changes and potential index of refraction changes due to changes in pressure. This mitigation strategy has been proven in similar applications/system.<sup>4</sup>

There have been some studies that have shown that doped silicon may have different thermal properties than pure silicon,<sup>35,36</sup> including different values of thermal expansion and conductivity. To decrease the deformation we describe in this paper, the coefficient of thermal expansion of the doped silicon would have to approach that of gold. This does not seem to be the case: the CTE of gold is  $\sim 14 \times 10^{-6} \text{ K}^{-1}$ , the CTE of pure silicon is  $\sim 3 \times 10^{-6} \text{ K}^{-1}$ , and the increase of silicon CTE due to doping was found to be of  $1 \times 10^{-8} \text{ K}^{-1}$ .<sup>36</sup> This shows that current doping techniques are not sufficient to increase the CTE of silicon enough; however, future research might bring promising results.

#### 4.5 Conclusions

The authors have presented experimental results of MEMS FSMs deformation when a laser beam is reflected by their surface. We have shown that the amount of induced focus error is directly proportional to the incident laser power (e.g., amount of absorbed heat). We have shown that there is not a strong enough correlation between the effect in ambient conditions versus under vacuum. We have obtained analytical results in Ansys that reach similar defocusing values as the experimental results, namely, up to 430 nm of peak to valley defocusing deformation when the mirrors are under vacuum and reflect a laser beam of 27 dBm (0.5 W). We suggest that future MEMS FSM users perform a Zemax analysis of their entire optical system, including the FSM. We have calculated that the impact of such deformations on a satellite communication link budget is  $\sim 10$  dBm, which could impact the communication link closure.

It is the authors' recommendation that a system with the described gold-coated MEMS FSMs should not exceed 200 mW (or 23 dBm) of optical power at 1550-nm incident laser light for continuous operation. Below this level of incident power, the absorbed heat (below 6 mW) is not yet enough to deform the mirror significantly, keeping the errors negligible and the overall impact inside the margins of a communication link budget.

## 5 Appendix A—Test Procedure

Both environment condition tests (ambient pressure and vacuum) follow the same procedure: capture the SFE with the Zygo interferometer, capture an infrared image of the mirror, and increase the laser power. Then, the sequence is repeated as power levels increase. The laser starts at 17 dBm of power then is increased to 20, 23, and 27 dBm. In some cases, the OD 1.0 neutral density filter is removed from the laser and its power is further increased to 30, 33, and 37 dBm. As explained further in Sec. 4.3.2, most mirrors would collapse when more than 30 dBm of laser was reflected at their surface. Hence to avoid catastrophic failure, we did not test most of

the mirrors above 27 dBm. This step-by-step description details the test procedure in ambient pressure and under vacuum:

At ambient pressure (101 kPa) and ambient temperature (~20°C):

1. Measure the baseline SFE of the DUT with the Zygo interferometer (with the laser turned off);
2. Capture the baseline thermal image of the DUT with the FLIR C3 (with the laser turned off);
3. Set the laser power to 17 dBm;
4. Measure the SFE of the DUT with the Zygo interferometer;
5. Capture a thermal image of the DUT with the FLIR C3;
6. Increase the laser power to 20 dBm and repeat steps 4 and 5;
7. Increase the laser power to 23 dBm and repeat steps 4 and 5;
8. Increase the laser power to 27 dBm and repeat steps 4 and 5;
9. Turn off the laser and repeat steps 4 and 5;
10. Stop the test.

At vacuum (below 8E-5 Torr) and ambient temperature (~20°C):

1. Measure the baseline SFE of the DUT with the Zygo interferometer (with the laser turned off and in ambient pressure);
2. Capture the baseline thermal image of the DUT with the FLIR C3 (with the laser turned off and in ambient pressure);
3. Turn on the vacuum pumps and wait until the vacuum level is below 5.0E-4 Torr;
4. Measure the vacuum baseline SFE of the DUT with the Zygo interferometer (with the laser turned off);
5. Capture the vacuum baseline thermal image of the DUT with the FLIR C3 (with the laser turned off);
6. Set the laser power to 17 dBm;

Serial # 5426  
Engineer PVP

Ambient test baseline			Vacuum @7.8E-5 Torr			Vacuum @5.7E-5 Torr		
Time (am)	Action	dBm	Time (pm)	Action	dBm	Time (pm)	Action	dBm
11:16	Power	0	1:40	Power	0	3:04	Power	0
11:16	Zygo		1:40	Zygo		3:04	Zygo	
11:17	FLIR		1:42	FLIR		3:06	FLIR	
11:21	Power	17	1:59	Power	27	3:07	Power	27
11:22	Zygo		2:00	Zygo		3:08	Zygo	
11:22	FLIR		2:00	FLIR		3:08	FLIR	
11:23	Power	20	2:01	Power	30	3:09	Power	30
11:24	Zygo		2:02	Zygo		3:10	Zygo	
11:24	FLIR		2:02	FLIR		3:10	FLIR	
11:25	Power	23	2:03	Power	31	3:11	Power	33
11:26	Zygo		2:04	Zygo		Mirror fell Off!		
11:26	FLIR		2:04	FLIR		3:15	Vacuum off	
11:27	Power	27	2:05	Power	37			
11:28	Zygo		2:06	Zygo				
11:28	FLIR		2:06	FLIR				
11:28	Power	0	2:06	Power	0			
11:29	Zygo		2:07	Zygo				
11:29	FLIR		2:07	FLIR				
11:33	Zygo		2:11	Zygo				
11:33	FLIR		2:11	FLIR				
11:38	Zygo		2:16	Zygo				
11:38	FLIR		2:16	FLIR				
Removed ND filter			Allowed mirror to cool down					
11:40	Vacuum on							

Fig. 7 Example test log.

7. Measure the SFE of the DUT with the Zygo interferometer;
8. Capture a thermal image of the DUT with the FLIR C3;
9. Increase the laser power to 20 dBm and repeat steps 4 and 5;
10. Increase the laser power to 23 dBm and repeat steps 4 and 5;
11. Increase the laser power to 27 dBm and repeat steps 4 and 5;
12. Turn off the laser and repeat steps 4 and 5;
13. Turn off the vacuum pumps, vent the system, and stop the test.

Figure 7 shows one test log in which the OD 1.0 filter was removed and the laser power was increased until 37 dBm. This DUT failed at 33 dBm of laser power, when the mirror fell off its base.

## Acknowledgments

We thank Facebook Connectivity Labs for funding this research. The author PVP was an intern PhD student at Facebook Connectivity Labs on the summer of 2019. There are no conflicts of interests.

## References

1. P. S. Salter and M. J. Booth, "Adaptive optics in laser processing," *Light Sci. Appl.* **8**, 110 (2019).
2. R. W. Kingsbury et al., "Fast-steering solutions for CubeSat-scale optical communications," *Proc. SPIE* **10563**, 105630G (2014).
3. V. Milanovic et al., "Compact MEMS mirror based Q-switch module for pulse-on-demand laser range finders," *Proc. SPIE* **9375**, 93750H (2015).
4. C. Chen et al., "Demonstration of a bidirectional coherent air-to-ground optical link," *Proc. SPIE* **10524**, 105240G (2018).
5. P. R. Yoder, Jr. and D. Vukobratovich, *Opto-Mechanical Systems Design*, 4th ed., Vol. **2**, Taylor & Francis Group, Boca Raton, Florida (2015).
6. J. A. Dobrowolski, "Optical properties of films and coatings," Chapter 42 in *Handbook of Optics*, M. Bass, Ed., 2nd ed., Vol. **1**, Photonics Research Group, pp. 42.1–42.130, McGraw Hill, New York (2010).
7. N. Sidqi et al., "Comparative study of dielectric coating materials for micro-cavity applications," *Opt. Mater. Express* **9**, 3452 (2019).
8. A. Rogalski and K. Chrzanowski, "Infrared devices and techniques (revision)," *Metrol. Meas. Syst.* **21**, 565–618 (2014).
9. B. Hu et al., "New design for highly durable infrared-reflective coatings," *Light Sci. Appl.* **7**, 17175 (2018).
10. Mirrorcle Technologies, Inc., "Gimbal-less single-axis and dual-axis (Tip-Tilt) MEMS mirrors," November 2019, <https://www.mirrorcletech.com/devices.html>.
11. Mirrorcle Technologies, Inc., "Mirrorcle technologies MEMS mirrors—technical overview," 2018, [https://www.mirrorcletech.com/pdf/MTI\\_MEMS\\_Mirrors\\_Technical\\_Overview.pdf](https://www.mirrorcletech.com/pdf/MTI_MEMS_Mirrors_Technical_Overview.pdf).
12. J. Zhang et al., "Thermal analysis of micromirrors for high-energy applications," *IEEE Trans. Adv. Packag.* **26**(3), 310–317 (2003).
13. S. K. Gokce et al., "A high-frequency comb-actuated resonant MEMS scanner for micro-displays," in *16th Int. Conf. Opt. MEMS and Nanophotonics*, IEEE, Vol. 11, p. 35 (2011).
14. C. Wolter et al., "Scanning 2D micromirror with enhanced flatness at high frequency," *Proc. SPIE* **6114**, 61140L (2006).
15. M. T. Hunwardsen, P. do Vale Pereira, and K. Cahoy, "Characterization of laser thermal loading on a MEMS FSM in vacuum," in *Int. Conf. Space Opt. Syst. and Appl.*, Portland (2019).
16. M. A. Krainak and D. M. Cornwell, "NASA optical communication strategy and technology," in *OSA—Adv. Photonics Cong.*, California (2019).

17. P. Serra et al., "Optical communications crosslink payload prototype development for the Cubesat laser infrared CrosslinK (CLICK) mission," in *33rd Annu. AIAA/USU Conf. Small Satellites*, Utah (2019).
18. V. N. Mahajan, "Optical systems with circular pupils," Chapter 8 in *Aberration Theory Made Simple*, Vol. **TT-6**, D. O'Shea, Series Ed., p. 74, SPIE Press, Bellingham, Washington (1991).
19. L. B. Stotts et al., "Free-space optical communications link budget estimation," *J. Appl. Opt.* **49**, 5333 (2010).
20. D. J. Schroeder, "Diffraction theory and aberrations," Chapter 10 in *Astronomical Optics*, 2nd ed., pp. 69–110, Elsevier Academic Press (2000).
21. C. Mafusire and A. Forbes, "Mean focal length of an aberrated lens," *J. Opt. Soc. Am. A* **28**, 1403–1409 (2011).
22. X. Zhang et al., "Analysis of defocus aberration characteristics on a typical passively confocal unstable resonator," *Optik* **202**, 163625 (2020).
23. C. Schulze et al., "Beam-quality measurements using a spatial light modulator," *Opt. Lett.* **37**, 4687–4689 (2012).
24. O. A. Schmidt et al., "Real-time determination of laser beam quality by modal decomposition," *Opt. Express* **19**, 6741–6748 (2011).
25. H. Jelinkova, Ed., "Laser characteristics," Chapter 2 in *Lasers for Medical Applications*, pp. 17–46, Woodhead Publishing, Philadelphia, Pennsylvania (2013).
26. R. E. Sheriff and A. R. L. Tatnall, "Telecommunications," Chapter 12 in *Spacecraft Systems Engineering*, P. Fortescue, G. Swinerd, and J. Stark, Eds., 4th ed., pp. 395–437, John Wiley & Sons, Ltd., West Sussex, United Kingdom (2011).
27. T. Takeshi et al., "Light commands: laser-based audio injection attacks on voice-controllable systems," 2019, <https://lightcommands.com>.
28. Y. Wang et al., "Optical properties and residual stress of YbF<sub>3</sub> thin films deposited at different temperatures," *Appl. Opt.* **47**, C319 (2008).
29. T. Begou and J. Lumeau, "Accurate analysis of mechanical stress in dielectric multilayers," *Opt. Lett.* **42**, 3217 (2017).
30. M. Bischoff et al., "Postdeposition treatment of IBS coatings for UV applications with optimized thin-film stress properties," *Appl. Opt.* **53**, A212 (2014).
31. M. Minissale et al., "The temperature dependence of optical properties of tungsten in the visible and near-infrared domains: an experimental and theoretical study," *J. Phys. D Appl. Phys.* **50**, 455601 (2017).
32. K. Soosaar, "Design of optical mirror structures," 1971, <https://ntrs.nasa.gov/search.jsp?R=19720016845>.
33. Y.-C. Chen et al., "Optimization of lightweight structure and supporting bipod flexure for a space mirror," *J. Appl. Opt.* **55**, 10382 (2016).
34. Y. Qu et al., "Lightweight design of multi-objective topology for a large aperture space mirror," *J Appl. Sci.* **8**, 2259 (2018).
35. C. Gayner et al., "Space strategy for exceptionally low thermal conductivity and high zT in antimony-doped bulk silicon," *Mater. Today Energy* **12**, 327 (2019).
36. B. S. Berry and W. C. Pritchett, "Stress and thermal expansion of boron-doped silicon membranes on silicon substrate," *J. Vac. Sci. Technol. A* **9**, 2231 (1991).

**Paula do Vale Pereira** is a PhD candidate in the Department of Aeronautics and Astronautics at MIT, specializing in the thermal and mechanical design of space exploratory probes and satellite payloads. She received her MS degree in space systems engineering from MIT in 2019, and her MS and BS degrees in mechanical engineering from the Federal University of Santa Catarina in 2017 and 2014, respectively.

**Matthew T. Hunwardsen** has been an electro-optic scientist for Facebook Connectivity Labs working on free-space optical communications since 2014. Previously, he worked at Rockwell Science Center in 2000 to 2006 on liquid crystal devices for laser beam steering, and then at Optical Physics Company in 2006 to 2014, leading development deformable mirrors for high energy lasers. He received his BS degrees in mathematics and physics

in 2001, and his MS degree in physics in 2005. He holds four patents and multiple publications.

**Kerri L. Cahoy** is an associate professor in the Department of Aeronautics and Astronautics at MIT. She received her BS degree in electrical engineering from Cornell University in 2000 and her MS and PhD degrees in electrical engineering from Stanford University in 2002 and 2008, respectively, working with the Radio Science Team on Mars Global Surveyor. She joined the MIT faculty in July 2011 and leads the Space Telecommunications, Astronomy, and Radiation Laboratory (STAR Lab).